

## Experimental demonstration of epsilon-near-zero water waves focusing

T. Bobinski, A. Eddi, P. Petitjeans, A. Maurel, and V. Pagneux

Citation: [Applied Physics Letters](#) **107**, 014101 (2015); doi: 10.1063/1.4926362

View online: <http://dx.doi.org/10.1063/1.4926362>

View Table of Contents: <http://scitation.aip.org/content/aip/journal/apl/107/1?ver=pdfcov>

Published by the [AIP Publishing](#)

---

### Articles you may be interested in

[On-chip focusing in the mid-infrared: Demonstrated with ring quantum cascade lasers](#)

Appl. Phys. Lett. **104**, 151105 (2014); 10.1063/1.4871520

[Loss-compensated broadband epsilon-near-zero metamaterials with gain media](#)

Appl. Phys. Lett. **103**, 201109 (2013); 10.1063/1.4831768

[Light focusing using epsilon-near-zero metamaterials](#)

AIP Advances **3**, 112124 (2013); 10.1063/1.4834435

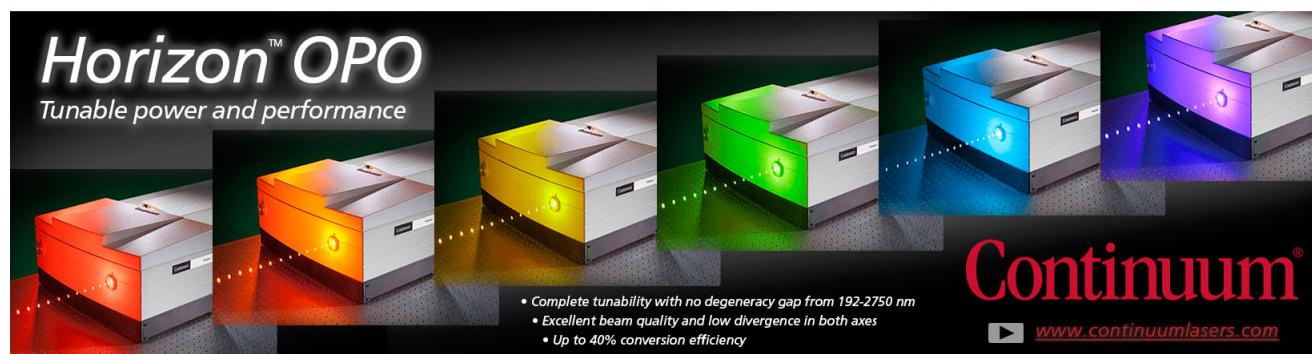
[Experimental realization of epsilon-near-zero metamaterial slabs with metal-dielectric multilayers](#)

Appl. Phys. Lett. **103**, 051111 (2013); 10.1063/1.4817678

[Ultra-broadband simultaneous superluminal phase and group velocities in non-Foster epsilon-near-zero metamaterial](#)

Appl. Phys. Lett. **102**, 054108 (2013); 10.1063/1.4790297

---

The advertisement for the Continuum Horizon OPO features a row of five laser units, each emitting a different colored beam (red, orange, yellow, green, blue) from its front. The units are sleek, rectangular, and silver-colored. The background is dark with a subtle grid pattern. The text 'Horizon™ OPO' is prominently displayed in the top left, with the tagline 'Tunable power and performance' below it. In the bottom right, the 'Continuum®' logo is shown in a large, stylized red font, with the website 'www.continuumlasers.com' underneath. A list of features is provided in the bottom center: 'Complete tunability with no degeneracy gap from 192-2750 nm', 'Excellent beam quality and low divergence in both axes', and 'Up to 40% conversion efficiency'. A small play button icon is also visible next to the website address.

# Experimental demonstration of epsilon-near-zero water waves focusing

T. Bobinski,<sup>1</sup> A. Eddi,<sup>1</sup> P. Petitjeans,<sup>1</sup> A. Maurel,<sup>2</sup> and V. Pagneux<sup>3</sup>

<sup>1</sup>Laboratoire de Physique et Mécanique des Milieux Hétérogènes (PMMH), UMR CNRS 7636, Ecole Supérieure de Physique et de Chimie Industrielles (ESPCI), Univ. P et M. Curie, Univ. D. Diderot, 10 rue Vauquelin, 75005 Paris, France

<sup>2</sup>Institut Langevin LOA, UMR CNRS 7587-ESPCI, 5 rue Jussieu, 75005 Paris, France

<sup>3</sup>Laboratoire d'Acoustique de l'Université du Maine, UMR CNRS 6613, Avenue Olivier Messiaen, 72085 Le Mans, France

(Received 12 March 2015; accepted 19 June 2015; published online 6 July 2015)

We explore an  $\epsilon$ -near-zero analogue for water waves using deep water and shallow water domains to obtain different phase velocities. Being inherently non linear, water waves permit to inspect focusing of harmonically generated waves. Experimental measurements show cascade of focal spots up to the fourth harmonic, allowing sub wavelength focusing with respect to the first harmonic wavelength. © 2015 AIP Publishing LLC. [<http://dx.doi.org/10.1063/1.4926362>]

Metamaterials have gained a lot of attention in wave physics in the last two decades, thanks to their prospective applications.<sup>1</sup> Among various newly designed materials, both  $\epsilon$ -near-zero (ENZ)<sup>2,3</sup> and refractive index-near-zero,<sup>4,5</sup> have made tailoring phase pattern feasible.<sup>6</sup> When an ENZ-material is used to fill a narrow channel connecting two larger waveguides, supercoupling can be observed.<sup>2</sup> In such a channel, wave energy is “squeezed” leading to strong increase of nonlinearities related to field enhancement.<sup>7</sup> When an ENZ material is used for wave front shaping, focusing can be easily obtained.<sup>6</sup> In this case, the ENZ material fills a lens shape region with a low refractive index (due to low permittivity  $\epsilon$  value) with respect to the reference medium where focusing will occur. In the context of water waves, where other types of metamaterials have been demonstrated,<sup>8–15</sup> an ENZ material can be achieved by means of regions with deep water surrounded by shallow water to generate the high contrast between the refractive indices. On the other hand, shallow water waves are non linear in usual conditions, thus, it is tempting to explore the influence of non linearities on the focusing expected in the linear regime; this is the subject of the present letter.

Let us consider an ENZ wave front shaping in the context of two dimensional propagation of electromagnetic waves with transverse magnetic polarization<sup>2</sup>

$$\nabla \left( \frac{1}{\epsilon} \nabla H \right) + \frac{\omega^2}{c_0^2} H = 0, \quad (1)$$

where  $H$  is the magnetic field,  $\omega$  is the frequency,  $c_0$  is the speed of light in a vacuum, and  $\epsilon$  is the relative permittivity. Considering a given leading edge with radius  $R$ , wave front shaping requires that the edge is an isophase for the incident wave<sup>6</sup> (meaning that  $R \ll \lambda_1$ ) and this implies that one needs to adjust the permittivity  $\epsilon_1$  in front of the edge. To focus the wave, the radius should also be larger than the wavelength in the exterior domain with permittivity  $\epsilon_2$ , yielding  $\epsilon_1/\epsilon_2 \ll 1$ . Therefore, focusing using ENZ wave front shaping can be realized by setting high contrast of permittivity between two adjacent domains. In the context of water waves, when the depth is much smaller than the wavelength ( $kh \ll 1$ ), the surface elevation  $\eta$  is described by the shallow-water (SW) approximation<sup>16</sup>

$$\nabla(h\nabla\eta) + \frac{\omega^2}{g}\eta = 0, \quad (2)$$

where  $h$  denotes the water depth at rest and  $g$  stands for the gravitational acceleration. Thus, it appears that, for shallow water, the wavenumber  $k_{SW}$  is given by  $k_{SW} = \omega/\sqrt{gh}$ . The analogy between Eqs. (1) and (2) and the correspondence  $1/\epsilon \leftrightarrow h$  indicates that ENZ wave front shaping can be achieved by means of water depth contrast  $h_{SW}/h_{DW} \ll 1$ . The upper limit of meaningful depth increase of  $h_{DW}$  is given by deep-water (DW) regime, with associated wavenumber  $k_{DW} = \omega^2/g$ .<sup>17</sup> Thus, the efficiency of the analogy is measured by the magnitude of  $k_{SW}/k_{DW} = \sqrt{\delta/h}$  with  $\delta = g/\omega^2$  the water wavelength scale.

Figure 1 shows the experimental realization of the water wave analogue of an ENZ lens within a waveguide. The lens has a semi circular shape of diameter  $d=200$  mm. Width of the waveguide is adjusted to the lens diameter. Taking into

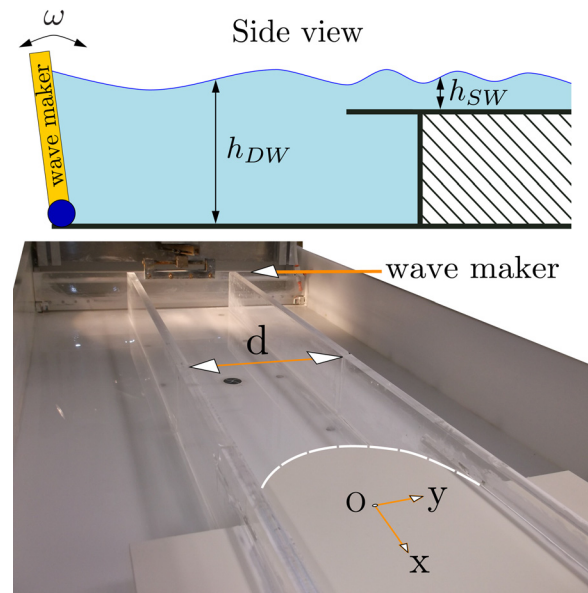


FIG. 1. Experimental setup of an ENZ lens for water waves. The lens has a semi circular shape (white dotted line) with diameter  $d=200$  mm and center O. It separates the shallow water region, with mean depth  $h_{SW} = 7$  mm, and the deep water region, with mean depth  $h_{DW} = 67$  mm. The lens is placed within a waveguide, whose width is adjusted to the lens diameter.

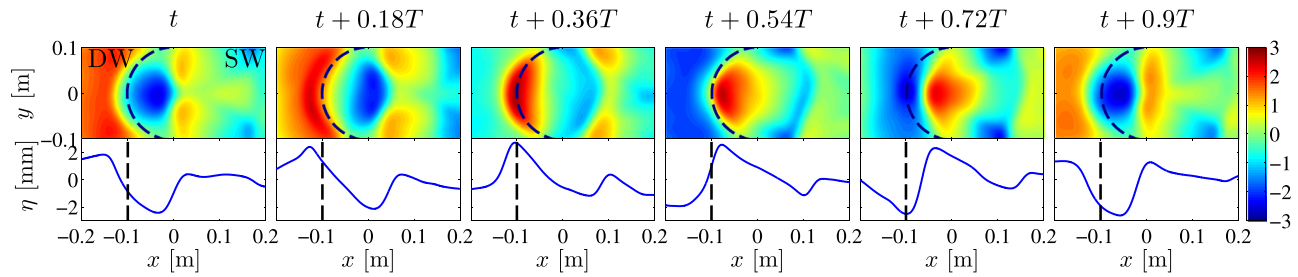


FIG. 2. Top panel: Typical temporal sequence of the measured surface elevation fields for  $\omega = 8.6 \text{ s}^{-1}$  and period  $T = 0.73 \text{ s}$ . SW and DW denote shallow-water and deep-water regions, with  $h_{\text{SW}} = 7 \text{ mm}$  and  $h_{\text{DW}} = 67 \text{ mm}$  water depth, respectively. The dashed-line indicates the position of the lens. The scale of colorbar is in millimeters. Bottom panel: corresponding profiles of the surface elevation at  $y = 0$ .

account, experimental constraints, such as bottom friction and size of the container, with a working frequency range being 1.4–2.1 Hz, we impose  $h_{\text{SW}} = 7 \text{ mm}$  in the shallow water region and the depth in deep water region is  $h_{\text{DW}} = 67 \text{ mm}$ , resulting in  $k_{\text{SW}}/k_{\text{DW}} \simeq 3$  (with wavelengths of 18 and 50 cm in the shallow and deep water, respectively). We generate waves by means of a paddle wave maker hinged at the bottom. Space time resolved measurements of the surface elevation field are performed using Fourier Transform Profilometry (FTP) technique, which has been adapted for water wave measurements (for details see Refs. 18, 19, and 30). Fringes are projected by a high-resolution projector ( $1920 \times 1080 \text{ pixels}^2$ ) and fields of the surface elevation are captured using a 4MPix camera with sampling frequency  $f = 15 \text{ Hz}$ . The area of the measured fields which is analyzed is  $0.4 \times 0.2 \text{ m}^2$ , covering both deep and shallow-water regions. The in-plane spatial resolution is governed by the size of the projected pixel, which is 0.39 mm, and the accuracy in the height detection is about 0.43 mm, determined by comparison with laser measurements. In Fig. 2, we present a typical temporal sequence of the surface elevation fields  $\eta(x, y, t)$  over a period  $T$ , and the corresponding profiles along the central line  $y = 0$  for frequency  $\omega = 8.6 \text{ s}^{-1}$  (the incident wave comes from the right). As expected, the wave has an almost uniform phase in the DW region. Next, in the SW region, the focusing is visible, with typical extension being comparable to the radius of the lens, in agreement with Rayleigh criterion in  $\lambda/2$ , and the wavelength  $\lambda = 18 \text{ cm}$  at this frequency.

As previously mentioned, shallow water waves are easily non linear, and a useful measure of the non linearity is the Ursell number  $U_r$ :  $U_r = A\lambda^2/h_{\text{SW}}^3$ , with  $A$  is the wave amplitude (linear waves being associated to  $U_r \ll 100$  (Refs. 20–22)). In our experiments, with  $A \sim 2 \text{ mm}$ , the non linear regime, qualitatively observed on the profiles reported in Fig. 2, is confirmed by large Ursell numbers  $U_r \sim 100 - 400$ . This is further quantified in Fig. 3, where we report the frequency spectrum of the surface elevation at the center of the circle ( $x = 0, y = 0$ ); the harmonics are significant, with an amplitude for the second harmonic at  $2\omega$  being about 30% of the first harmonic, and visible peaks until the fourth harmonic. From here on, we inspect quantitatively how the non linearities affect the focusing expected in the linear regime. Therefore, we extract the fields of each harmonic from the experimental data, expanding the measured  $\eta(x, y, t)$  into a Fourier series

$$\eta(x, y, t) = \sum_n \hat{\eta}_n(x, y) e^{in\omega t}, \quad (3)$$

where  $\hat{\eta}_n(x, y) = \frac{1}{T} \int_0^T dt \eta(x, y, t) e^{-in\omega t}$ . The complex field  $\hat{\eta}_n(x, y)$  corresponds to the  $n$ -th harmonic (for  $n > 0$ ) of the fundamental  $\omega$ .

Figure 4 shows the main results of our study. We report the spatial fields of the wave intensity for the total field  $I(x, y) = \max_{t \in [0, T]} \eta^2(x, y, t)$  and for each harmonic  $I_n(x, y) = |\hat{\eta}_n(x, y)|^2$  ( $n = 1, 2, 3, 4$ ), at two different frequencies  $\omega_1 = 9.86 \text{ s}^{-1}$  and  $\omega_2 = 12.39 \text{ s}^{-1}$ . The first striking point is that the wave does not follow typical ENZ focusing, being slightly shifted from the expected focal point. Indeed, constant phase at the lens should result in the focal point at the center of the circular edge. Rather, the observed focal spot is located in front of the center of the circle. This is a kind of negative refraction effect that might be ascribed to non linearities. Second, and more surprisingly, the successive harmonics appear to be more and more focused. This is quantified in Fig. 5, where we report the characteristics of the focal spots in terms of their axial and lateral extensions  $L_x$  and  $L_y$ , the axial position  $X$  of their maximum intensity  $I_{\text{max}}$ , and their contrast  $I_{\text{max}}/\bar{I}$  (with  $\bar{I}$  the mean intensity). The contrasts of the focal spots appear to be roughly the same for all the harmonics, while both the position of focalization and the focal spot sizes present a variation when increasing the order of the harmonic. First, higher harmonics tend to focus closer to the center of the circle, but always in front of the expected ENZ focal point of the lens. This confirms the negative refraction type effect. On the other hand,

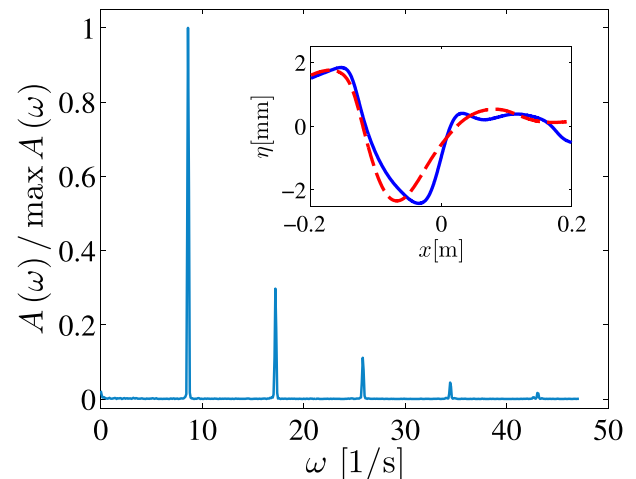


FIG. 3. Temporal spectrum obtained at the center of the circle for  $\omega = 8.6 \text{ s}^{-1}$ . The inset presents instantaneous elevation field at  $y = 0$  (solid blue line) and corresponding linear component (dashed red line).



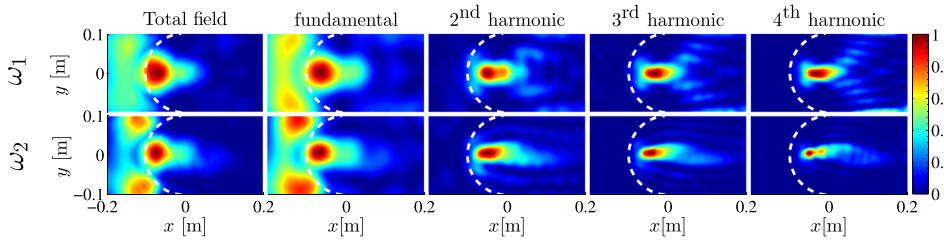


FIG. 4. Normalized intensity of the wave field ( $I/I_{\max}$ ) for  $\omega_1 = 9.86 \text{ s}^{-1}$  and for  $\omega_2 = 12.39 \text{ s}^{-1}$ . The dashed line represents the position of the lens. The scale bar (in the top left figure) corresponds to 0.1m.

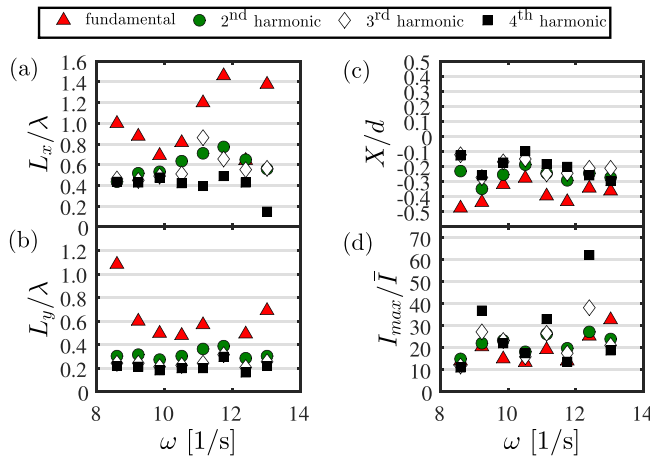


FIG. 5. Focal spot parameters: (a) horizontal  $L_x/\lambda$  extension of the focal spot, (b) vertical  $L_y/\lambda$  extension of the focal spot, (c) horizontal position of the focal spot  $X/d$  as a function of  $\omega$ , where  $d$  denotes lens diameter, (d) contrast  $I_{\max}/\bar{I}$ .  $L_x$  and  $L_y$  are determined as a distance between the points near the maximum intensity, for which the intensity  $I_n$  equals  $\max I_n/2$ . Contrast is defined as  $I_{\max}/\bar{I}$ , where  $I_{\max}$  and  $\bar{I}$  denote maximum amplitude and mean value of the amplitude in the far-field for  $x$  in the range  $[0.17, 0.2]$  m.

the size of the focal spots tends to decrease. As previously mentioned, for the fundamental component,  $L_x$  and  $L_y$  reasonably follow the Rayleigh criterion. For the higher  $n$ -th harmonic, it appears that the focal spot size follows a sub-wavelength scaling  $\lambda/n$ , a size corresponding to the wavelength of the harmonic  $n\omega$  in the non dispersive part of the dispersion relation.<sup>17</sup>

These facts reveal that the higher order harmonics are not localized only where the fundamental has large amplitude. This suggests that they are not simply slave to the fundamental and this is illustrated in Fig. 6. Indeed, in the weakly nonlinear regime, if we neglect forcing by the fundamental, the harmonics satisfy the Helmholtz equations<sup>23</sup>

$$(\Delta + k_n^2)\hat{\eta}_n(x, y) = 0, \quad (4)$$

where  $k_n$  is the wavenumber associated to  $n\omega$ , i.e.,  $D(n\omega, k_n) = 0$ , where  $D(\omega, k) = \omega^2 - gk \tanh(kh)(1 + \gamma k^2/\rho g)$  is the

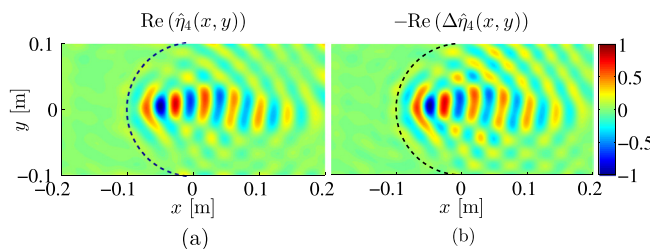


FIG. 6. Normalized amplitude of (a)  $\hat{\eta}_4$  real part and (b) its Laplacian for  $\omega = 12.39 \text{ s}^{-1}$  (see 4th harmonic for  $\omega_2$  in Fig. 4). Dashed line represents the position of the lens. Estimated wavenumber is  $k_4 = 184 [1/\text{m}]$ .

water wave dispersion relation (and note that  $k_n \simeq nk$  only in the non dispersive part of the dispersion relation). A harmonic which is solution to this equation is called a free-wave—in contrast to bound-waves which are slave to the fundamental. In the example of Fig. 6, it is experimentally demonstrated<sup>24</sup> that  $\Delta \hat{\eta}_4 = -k_4^2 \hat{\eta}_4$ , implying free-wave behavior in this case. Analysis of other harmonics reveals the presence of bound-waves as well. Thus, the observed focusing of the harmonics cannot be attributed either to a pure free wave behavior or to a pure bound wave behavior.

In summary, metamaterials are promising for the control of water wave propagation, for which several demonstrations have been presented in the linear regime.<sup>8–10,12,15</sup> Nevertheless, water waves are inherently nonlinear, which gives rise to several surprising effects.<sup>25–27</sup> In this letter, using metamaterial concepts and intrinsic water wave non linearities, we report the effect of sub-wavelength harmonic focusing with respect to the incident wavelength. Additionally, in contrast to gradient index lenses for water waves,<sup>13,14,28,29</sup> our result show how to obtain a topographical lens from a sudden change of depth, owing to the ENZ concept.

The authors acknowledge the financial support of the Agence Nationale de la Recherche through the Grant No. DYNAMONDE ANR-12-BS09-0027-01.

<sup>1</sup>N. Engheta and R. W. Ziolkowski, *Metamaterials: Physics and Engineering Explorations* (John Wiley & Sons, 2006).

<sup>2</sup>M. Silveirinha and N. Engheta, *Phys. Rev. Lett.* **97**, 157403 (2006).

<sup>3</sup>B. Edwards, A. Alù, M. Young, M. Silveirinha, and N. Engheta, *Phys. Rev. Lett.* **100**, 033903 (2008).

<sup>4</sup>S. Kocaman, M. S. Aras, P. Hsieh, J. F. McMillan, C. G. Biris, N. C. Panoiu, M. B. Yu, D. L. Kwong, A. Stein, and C. W. Wong, *Nat. Photonics* **5**, 499 (2011).

<sup>5</sup>E. J. R. Vespeur, T. Coenen, H. Caglayan, N. Engheta, and A. Polman, *Phys. Rev. Lett.* **110**, 013902 (2013).

<sup>6</sup>A. Alù, M. Silveirinha, A. Salandrino, and N. Engheta, *Phys. Rev. B* **75**, 155410 (2007).

<sup>7</sup>C. Argyropoulos, P.-Y. Chen, G. D'Aguanno, N. Engheta, and A. Alù, *Phys. Rev. B* **85**, 045129 (2012).

<sup>8</sup>X. Hu and C. Chan, *Phys. Rev. Lett.* **95**, 154501 (2005).

<sup>9</sup>M. Farhat, S. Enoch, S. Guenneau, and A. B. Movchan, *Phys. Rev. Lett.* **101**, 134501 (2008).

<sup>10</sup>C. P. Berraquero, A. Maurel, P. Petitjeans, and V. Pagneux, *Phys. Rev. E* **88**, 051002 (2013).

<sup>11</sup>C. Zhang, C. T. Chan, and X. Hu, *Sci. Rep.* **4**, 6979 (2014).

<sup>12</sup>R. Porter and J. N. Newman, *J. Fluid Mech.* **750**, 124 (2014).

<sup>13</sup>Z. Wang, P. Zhang, X. Nie, and Y. Zhang, *Europhys. Lett.* **108**, 24003 (2014).

<sup>14</sup>R. B. Elandt, M. Shakeri, and M.-R. Alam, *Phys. Rev. E* **89**, 023012 (2014).

<sup>15</sup>H. Chen, J. Yang, J. Zi, and C. T. Chan, *Europhys. Lett.* **85**, 24004 (2009).

<sup>16</sup>J. Lighthill, *Waves in Fluids* (Cambridge University Press, 2001).

<sup>17</sup>The complete dispersion relation is given as  $\omega^2 = gk \tanh(kh)(1 + \gamma k^2/\rho g)$ , where  $\rho$  and  $\gamma$  denote water density and surface tension, respectively.

- <sup>18</sup>P. J. Cobelli, A. Maurel, V. Pagneux, and P. Petitjeans, *Exp. Fluids* **46**, 1037 (2009).
- <sup>19</sup>A. Maurel, P. Cobelli, V. Pagneux, and P. Petitjeans, *Appl. Opt.* **48**, 380 (2009).
- <sup>20</sup>M. Dingemans, *Water Wave Propagation Over Uneven Bottoms: Linear wave propagation*, Advanced Series on Ocean Engineering (World Scientific Publishing, 1997).
- <sup>21</sup>R. Dean and R. Dalrymple, *Water Wave Mechanics for Engineers and Scientists*, Advanced Series on Ocean Engineering (World Scientific, 1991).
- <sup>22</sup>C. Mei, M. Stiassnie, and D. Yue, *Theory and Applications of Ocean Surface Waves: Nonlinear Aspects*, Advanced Series on Ocean Engineering (World Scientific, 2005).
- <sup>23</sup>K. Belibassakis and G. Athanassoulis, *Coastal Eng.* **58**, 337 (2011).
- <sup>24</sup>To find wavenumber  $k_n$  from a given complex pattern  $\hat{\eta}_n(x, y)$ , the norm function  $||(\Delta + k_n^2)\hat{\eta}_n||$  is minimized in the complex plane  $k_n$ .<sup>30</sup> The discrete Laplacian is calculated as  $[\Delta\hat{\eta}]_{i,j} = \frac{1}{\Delta x^2} (\hat{\eta}_{i-1,j} + \hat{\eta}_{i+1,j} + \hat{\eta}_{i,j-1} + \hat{\eta}_{i,j+1} - 4\hat{\eta}_{i,j})$ .
- <sup>25</sup>A. Chabchoub and M. Fink, *Phys. Rev. Lett.* **112**, 124101 (2014).
- <sup>26</sup>H. Hennig, *Physics* **7**, 31 (2014).
- <sup>27</sup>J. Fouque and A. Nachbin, *Multiscale Model. Simul.* **1**, 609 (2003).
- <sup>28</sup>R. W. Whalin, *Coastal Eng. Proc.* **1**(12) (1970), see <http://journals.tdl.org/icce/index.php/icce/article/view/2766/2430>.
- <sup>29</sup>L. Griffiths and R. Porter, *Appl. Ocean Res.* **34**, 150 (2012).
- <sup>30</sup>A. Prasadka, B. Cabane, V. Pagneux, A. Maurel, and P. Petitjeans, *Exp. Fluids* **52**, 519 (2012).